Available online at www.sciencedirect.com
SCIENCE DIRECT
Journal of the European Ceramic Society 26 (2006) 2561–2579
www.elsevier.com/locate/jeurceramsoc

Plasma-sprayed graded ceramic coatings on refractory materials for improved chemical resistance

G. Bolelli, V. Cannillo, C. Lugli, L. Lusvarghi *, T. Manfredini

Dipartimento di Ingegneria dei Materiali e dell'Ambiente, Facoltà di Ingegneria, Università di Modena e Reggio Emilia, Via Vignolese 905, 41100, Modena, Italy

Received 11 March 2005; received in revised form 20 July 2005; accepted 31 July 2005
Available online 12 September 2005

Abstract

Plasma-sprayed ceramic coatings were manufactured on sintered alumina–mullite refractory bricks to improve their chemical resistance to molten glass. Mullite and alumina powders were employed. Graded layered coatings were designed and produced, to reduce the thermal expansion mismatch with the substrate: in all cases, the upper layer consisted in pure alumina (very resistant to chemical attack); alumina–mullite intermediate layers were added to match the low thermal expansion of the porous substrates. Plasma-sprayed coatings definitely improved both the abrasion resistance and the chemical resistance to long-time (8 h at 1400 °C) contact with molten glass, since the coating preserved its original microstructure. However, in thermal shock tests, some transverse cracks appeared; thus, thermal cycling tests in presence of molten glass indicated that, after a few cycles, the glass can penetrate down to these cracks. The tested samples were studied by means of scanning electron microscopy (SEM) with energy dispersive spectrometry (EDS) and X-ray diffraction (XRD).

Keywords: Chemical properties; Thermal shock resistance; Wear resistance; Refractories; Plasma spraying; Coatings

1. Introduction

Thermal spraying techniques are well known production routes for thermal and chemical resistant coatings.[1–3] Compared to other coating processes, thermal spraying techniques allow the deposition of very thick coatings (up to 1 mm or more),[1,4,5] a wide choice in coating materials (metals and alloys, oxide and non-oxide ceramics, composite materials),[5,6] relatively short production times, and automation of the coating process. In fact, they usually consist in melting and accelerating powder particles towards a substrate by means of a hot gas jet[7]; thus, the only requirement is that the coating material must have a stable liquid phase in a sufficiently large temperature range, without thermal dissociation or vaporization. Plasma-spraying is a particular thermal spraying technique where the hot jet accelerating the particles is a plasma jet, produced by a dc electric arc struck between a tungsten cathode and a water-cooled copper anode across a plasma-forming gas flow (generally consisting of a mixture of a primary gas like Ar and a secondary gas like H_2) inside a plasma torch. The exceptionally high temperatures which a plasma can reach (up to 15000 °C in its core) allow virtually any material to be melted and, consequently, to be employed as a coating material.[4,6,7] In particular, plasma spraying is very suitable for the production of pure ceramic coatings. Thus, because of the good thermal stability and chemical resistance of many ceramics, plasma spraying is widely employed in the manufacturing of thermal barrier coatings, which must stand very hot gas flows and provide thermal insulation to the substrate.[1] Thermally sprayed coatings with high-temperature chemical resistance requirements have often been considered for applications such as internal combustion engines (gas turbine engines and reciprocating endothermal engines), burners and waste incinerators.[8–10] However, the contact with chemically aggressive molten materials at high temperature and the simultaneous presence of mechanical actions due to convec-

* Corresponding author. Tel.: +39 0592056206; fax: +39 0592056243.
E-mail address: lucalusv@unimore.it (L. Lusvarghi).

0955-2219/$ – see front matter © 2005 Elsevier Ltd. All rights reserved.
doi:10.1016/j.jeurceramsoc.2005.07.066

tive flows or stirring devices, which occur in molten materials processing plants (glass manufacturing plants, primary metallurgy plants), require some components to tolerate an even more aggressive environment than those above mentioned. Thermally sprayed coatings have seldom been tested under these very demanding conditions.[11,12] In some cases, thermally sprayed Pt coatings have been proposed for the glass industry: Pt is renown for its chemical stability in almost every environment, but such coatings are, obviously, extremely expensive.[13] Mo and its alloys are also employed, but their use is limited to some water-cooled components[13]; besides, the dissolution of metal ions in the glass may alter its optical properties, which is an unacceptable drawback in many glass applications.

In particular, molten glass processing furnaces generally require the employment of very expensive electrofused alumina–zirconia–silica refractories in order to bear the chemical action of molten glass.[14] Sintered ceramics (which would cost up to 15–20 times less) are also employed in such applications, but the glass quickly infiltrates the pores and starts dissolving the material much faster, eventually disrupting the refractory. If a low porosity, chemically resistant, thick pure alumina coating could be deposited onto the surface of a sintered refractory brick, it would significantly hinder molten glass percolation and consequent refractory dissolution. Thus, coated sintered refractories could, at least partly (because structural mechanical resistance must be taken into account as well), replace the expensive electrofused ones. It should be considered that surface regeneration of worn component by thermal spraying is also possible: after a simple grit-blasting operation, new coatings can be deposited onto the worn surface. Being thermal spray torches relatively small and easy to handle (they could even be hand-operated), they could be employed for refractories regeneration inside the melting furnace, avoiding or retarding the extremely expensive, difficult and time-consuming furnace dismantling operation.

In this study, some low cost alumina–mullite sintered refractories were coated by means of plasma spraying, aiming at the production of a pure alumina top coating. Although pure alumina would show excellent chemical resistance in contact with many molten materials (not only glass, but also molten Al for instance), pure alumina sintered refractories are expensive because alumina cannot be sintered in a low-cost atmospheric pressure sintering process; hot pressing techniques are required which are obviously not easily applicable to a refractories mass production. However, since alumina possesses a higher thermal expansion coefficient (CTE) than common alumina–mullite based porous refractories, if a pure alumina layer was directly sprayed onto the refractory substrate huge thermal expansion mismatch stresses would arise. To lessen this trouble, graded coatings have been designed: underlying alumina–mullite layers have been sprayed before the alumina top coat, to exploit the thermal expansion coefficient of mullite. A mullite-containing top coat has never been considered, since mullite possesses definitely lower chemical resistance than alumina. Graded plasma-sprayed thermal barrier coatings have already been considered in several articles,[15–19] but they were not tested under very corrosive environments, and they always consisted of a metal–ceramic system, whereas a ceramic–ceramic graded coating is considered in the present research.

2. Materials and characterization

2.1. Substrates and coating production

Two different commercial alumina–mullite based sintered refractories, with commercial designation EP and EXTRA55, supplied as (220 mm × 110 mm × 60 mm) bricks, were employed in this study. Their nominal chemical composition and physical characteristics are listed in Table 1. Mechanical dilatometry (DIL 404, Netzsch, 10 °C/min heating up to 1200 °C) has been performed in order to assess the thermal expansion coefficient, which is a key parameter for the choice of the coatings layers sequence. Furthermore, they have been characterized through X-rays diffraction (PW 3710, Philips, Cu Kα radiation), SEM (Philips XL40), and mercury porosimetry (Micromeritics Autopore II 9215), in order to determine the actual porosity value.

Three commercially available thermal spray ceramic powders have been employed for coatings production: a $-45+15$ μm mullite powder (Saint Gobain #1020), a $-45+15$ μm alumina powder (Saint Gobain #153PT) and a $-31+3.5$ μm alumina powder (Sulzer Metco 105SFP). The powder characteristics have been checked by means of SEM imaging, X-rays diffraction and particle size measurement (Particle Sizer Analysette 22, Fritsch). The coatings have been plasma-sprayed in air plasma spraying (APS) mode, with a C.A.P.S. plant equipped with a Sulzer Metco F4-MB plasma torch with a 6 mm diameter nozzle (C.S.M. S.p.A., Rome, Italy, co-shared with Università La Sapienza, Rome, Italy). Spray parameters are listed in Table 2. The substrates were (110 mm × 60 mm × 10 mm) refractory plates, cut from the sintered bricks. A literature study has proven that the roughness of a sintered refractory allows proper coating adhesion[12] without any pre-deposition treatment step: however, in this case, the substrates surfaces have been altered by the cutting operation. Thus, grit blasting was performed, with alumina grits (Sulzer Metco Metcolite-C) and a vacuum

Table 1
Nominal chemical and physical properties of employed refractory substrates

Nominal properties	EP	EXTRA55
Nominal chemical composition		
Al_2O_3	37%	55%
SiO_2	58%	40%
Fe_2O_3	1.9%	2%
Impurities	Bal.	Bal.
Compressive strength (kg/cm^2)	500	550
Maximum working temperature (°C)	1360	1475

Table 2
Plasma-spraying parameters

Diameter and position of powder injector	1.5 mm internal diameter; 7 mm distance from torch axis; 6 mm distance from torch nozzle
Plasma gases flow rates	Ar: 45 Slm for 30 vol.% mullite layer in two-layered coatings; 50 Slm in all other cases; H_2:15 Slm
Voltage (V) × current (A)	65 V × 600 A (alumina layer); 73 V × 690 A (30 vol.% mullite layer in two-layered coatings); 65 V × 630 A (in all other cases)
Deposition distance	105 mm (30 vol.% mullite layer in two-layered coatings); 100 mm (in all other cases)
Torch traverse speed	500 mm/s

Note: Slm: standard litre per minute; 1 Slm = (1/6) × 10^{-4} S m^3/s.

operated hand-held blasting gun. A double feeding apparatus was employed for the alumina–mullite mixed layers production, the two pure ceramic powders being simultaneously fed into the plasma jet with the desired flow, in order to achieve the proper layer composition. To take into account the different flowability and deposition efficiency of the two different powders, preliminary tests were performed, spraying (with a fixed number of torch passes) pure alumina and pure mullite coatings with the same torch parameters employed in the composite layers deposition: to get the optimal tailoring of the layers, the ratio between the thicknesses of the two coatings was used to adjust the feeding parameters. The reliability of this method has already been demonstrated in a previous work.[20] The employment of a double feeder apparatus enables a great flexibility in the number and composition of layers with minimum time expenditure, whereas the use of pre-mixed powders in a single feeder would limit the choice in layers composition and cause a great time consumption because of repeated feeder unloading/reloading with the proper powder.

Two series of coatings were produced: the first one consists in two-layered coatings, the low number of layers being intended to minimize the coating cost; the second one consists in three-layered coatings on EXTRA55 substrates and four-layered ones on EP substrates, in order to lower thermal expansion coefficient mismatches between different layers. More layers were employed for the EP substrate because, as the results section will show, it possesses lower thermal expansion coefficient, thus it is more likely to cause thermal expansion mismatch troubles. Details of the layers composition are given in Table 3.

The composite layers were produced using the coarser alumina powders, because powders with a grain size distribution as similar as possible must be used in the production of plasma-sprayed composite coatings in order to achieve a homogeneous phases distribution, as shown by former studies.[20] The finer alumina powder, instead, was employed in the production of the top coating, in order to achieve the lowest possible porosity and minimum pore dimensions: the higher the top coating compactness, the better its chemical resistance and its barrier effect against molten material percolation. Details of feeding parameters are given in Table 4.

2.2. Microstructural characterization and abrasion resistance

Cross-sectional coating samples were cut from the coated refractories, cold-mounted in resin, ground with 400, 800, 1000 mesh SiC papers, polished with 3 μm and 0.5 μm diamond paste and observed through SEM. Image analysis was performed on 400× and 1000× SEM micrographs (UTHSCSA Image Tool 3.0) to assess the porosity; image analysis was also performed on SEM micrographs of refractories

Table 3
Layers composition

	1st layer	2nd layer	3rd layer	4th layer
Two-layered coating (1st series)	100% Alumina	70 vol.% Alumina, 30 vol.% mullite	None	None
Three-layered coating (2nd series, EXTRA55 substrate)	100% Alumina	70 vol.% Alumina, 30 vol.% mullite	35 vol.% Alumina, 65 vol.% mullite	None
Four-layered coating (2nd series, EP substrate)	100% Alumina	70 vol.% Alumina, 30 vol.% mullite	35 vol.% Alumina, 65 vol.% mullite	100% Mullite

Table 4
Feeding parameters for layered coatings

	Top alumina layer	30 vol.% mullite layer (in two-layered coatings, 1st spray run)	65 vol.% mullite layer	Pure mullite layer
Alumina powder/disk revolution speed/carrier gas flow	Metco 105SFP/12 rpm/Ar 3.5 Slm	S.G. #153PT/8.4 rpm/Ar 3.3 Slm	S.G. #153PT/4.2 rpm/Ar 3.3 Slm	
Mullite powder/disk revolution speed/carrier gas flow	–	S.G. #1020/3 rpm/Ar 3.3 Slm	S.G. #1020/6.5 rpm/Ar 3.3 Slm	S.G. #1020/10 rpm/Ar 3.3 Slm

Note: The same feeding parameters were employed for the 30 vol.% mullite layer in two-, three- and four-layered coatings.

to ascertain the reliability of the technique by comparison with the mercury porosimetry results. X-ray diffraction was performed on the upper and lower surfaces of the coatings to determine the crystalline phases; diamond papers were employed to ground the substrate away from the coating lower surface.

Since refractories (and, more generally, components designed to process molten materials) are also subject to wear, as formerly mentioned, dry particle abrasion resistance of both coated and uncoated samples was tested by means of a dry particles—steel wheel test (Ceramic Instruments AP/87), with a Fe360 steel wheel rotated at 75 rpm and pressed by a 40.2 N normal load against the sample surface in presence of a tangential flux (1 g per disk revolution) of corundum particles (FEPA 80: 180 μm mean particle diameter). The results are expressed as wear volume per unit sliding distance of the disk (mm^3/m). Although the test is carried out at room temperature, while the materials undergo mechanical loading at high temperature, the results can give useful qualitative indications about the performances of the different materials.

2.3. Thermal shock resistance

All the coatings were subjected to cyclic thermal shock testing: five (60 mm × 20 mm × 10 mm) samples (numbered from 1 to 5) were cut from the coated plates, heated in an electric kiln at 15 °C/min up to 1400 °C for the EXTRA55 substrate and 1300 °C for the EP substrate, left at 1400 °C or 1300 °C for 30 min, rapidly extracted and left in air at room temperature for 30 min in order to cool them down completely. Two different operating temperatures were chosen because of the different operating temperature upper limits of the two materials. Sample number 1 was then removed and analysed, while the others were subjected to further thermal shocks by inserting them into the kiln (which has been left at the chosen operating temperature) for 30 min and pulling them out again, that is at room temperature. The number of the sample corresponds to the number of the thermal cycles performed on it (up to 5). The thermally shocked samples were visually inspected to determine the presence of macroscopic cracks; cross-sectional SEM samples were then obtained as above described: SEM observation allowed further characterization of sample cracking and inspection of the modifications in the coating microstructure. X-ray diffractometry was also performed on both the upper and lower surfaces of the coatings, in order to verify the occurrence of phase transitions.

To interpret the experimental observations and get a better understanding of the thermal shock behaviour of the layered systems, a modified rule of mixtures approach[21] was adopted to qualitatively estimate the thermal expansion coefficients of alumina–mullite composite layers. Even though such approach has very limited accuracy for the present case, it can be useful in obtaining a rough qualitative estimate of the thermal behaviour of the various layers. The modified rule of mixtures law employed in this study is:

$$\alpha_c = \frac{E_{alumina}\,\alpha_{alumina}\,V_{alumina} + E_{mullite}\,\alpha_{mullite}\,V_{mullite}}{E_{alumina}\,V_{alumina} + E_{mullite}\,V_{mullite}} \quad (1)$$

where α_c = thermal expansion coefficient of the composite layer ($°C^{-1}$); $E_{alumina}$, $E_{mullite}$ = Young's moduli of the single constituents (GPa); $\alpha_{alumina}$, $\alpha_{mullite}$ = thermal expansion coefficient of the single constituents ($°C^{-1}$); $V_{alumina}$, $V_{mullite}$ = volume fraction of the constituents.

Since the elastic moduli and thermal expansion coefficients of thermally sprayed materials often differ significantly from those of corresponding massive materials,[22] they have been directly measured on free-standing plasma-sprayed alumina and mullite samples, deposited using the same parameters as the formerly described coatings.

As thermal shock testing involved high-temperature treatments (1300 °C and 1400 °C isotherms), it has been assumed that the most significant stresses were developed during cooling: at such very high temperatures, indeed, stress relaxation through creep becomes possible. Therefore, the thermomechanical properties which must be employed in the above formula are those of thermally treated coatings, which may possess relevant differences from those of untreated coatings due to the occurrence of a significant degree of microstructural (i.e. sintering) and structural (i.e. phase transformation) changes,[23,24] which shall be highlighted in Section 3. Thus, plasma-sprayed alumina and mullite self-standing samples were subjected to a 1400 °C thermal treatment before elastic modulus and thermal expansion coefficient measurement. The elastic modulus has been measured by depth sensing Vickers microindentation (MicroCombi Tester, CSM Instruments, Switzerland: 1 N indentation load, 0.8 N/min loading and unloading rate, 15 s loading time) on free-standing coatings cross-sections, mounted in resin and polished; the Oliver–Pharr formula[25] has been employed. An average of 20 measurements has been used in all cases. For reference, the elastic modulus of the as-sprayed self-standing samples (before the heat treatment) has also been measured. The CTE has been measured by a recently patented non contact optical dilatometer (Misura ODLT, Expert System Solutions, Modena, Italy; Fig. 1). Thin rectangular (50 mm × 10 mm × 1 mm) samples are placed into a furnace with their extremities illuminated by two beams of light; two digital cameras continuously monitor the extremities position during sample heating and record the thermal expansion curve, from which the thermal expansion coefficient can be calculated. The furnace heating rate is 10 °C/min up to a maximum temperature of 1150 °C.

2.4. Chemical resistance

The chemical resistance of coatings to molten glass was also tested. A frit employed in metals glazing, chemically very aggressive due to the presence of significant amounts of Na_2O, CaO, NiO, MnO_2, Fe_2O_3, ZnO, CoO, was used. Pow-

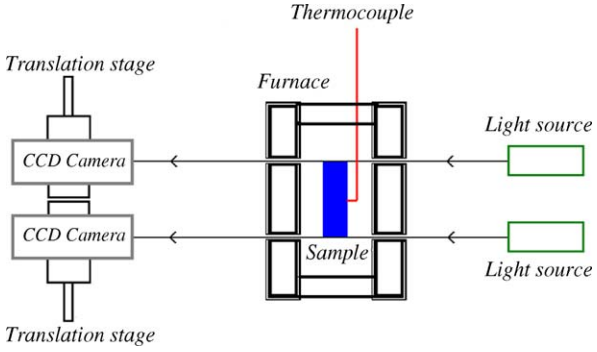

Fig. 1. Schematics showing the dilatometer used for the measurement of the coefficients of thermal expansion of alumina and mullite self standing samples.

ders obtained by ball milling the frit were laid onto a coated sample; the sample was then put into an electric kiln, heated up to 1400 °C (EXTRA55 substrate) or 1300 °C (EP substrate) at 15 °C/min, left at the operating temperature for 8 h, then slowly cooled down inside the kiln. The samples were visually inspected, then cut, mounted in resin, and observed through SEM to assess the actual frit penetration inside the coating. Uncoated refractory samples were also tested for reference.

To assess the combined effect of thermal cycling and chemical attack, the coatings on EXTRA55 substrate were also subjected to a combined test: before each thermal cycle, a certain amount of glass powder was laid on the coating. The thermo-chemically cycled samples were visually inspected, observed through SEM and subjected to X-ray diffractometry.

3. Results and discussion

3.1. The characterization of powders and substrates

Table 5 summarizes the powder characteristics. Particle size ranges measurements are very similar to the nominal values, although the coarser alumina powder possesses a higher average particle diameter than nominally declared. It is important to notice that the powders have a quite narrow particle size distribution, as it is required for the proper optimisation of parameters.

X-ray diffractometry indicated that α-Al_2O_3 and mullite ($3Al_2O_3{\cdot}2SiO_2$) are the main crystalline phases present in both refractory substrates employed; cristobalite (a crystalline phase of SiO_2 which is metastable at room temperature) is also present in EP substrates, some cristobalite and zircon exist in the EXTRA55 substrate. SEM micrographs show that these materials are very porous and heterogeneous, with large grains separated by huge voids (Fig. 2A and B), clearly indicating sintering difficulties due to the refractory nature of these compounds. In particular, the micrographs indicate the presence of large alumina grains (some of them are indicated by white arrows in Fig. 2A and B) poorly bonded to the surrounding material.

Table 5
Spray powders characteristics

Powder	Appearance and manufacturing	Nominal chemical composition	Phases (from XRD)	Particle size distribution
Fine alumina, Metco 105SFP (−31 + 3.5 μm nominal)	Angular, fused and crushed	Al_2O_3 99.89 wt%, NaO 0.09 wt.%, Fe_2O_3 0.01 wt.%, SiO_2 0.01 wt%	α-Al_2O_3	<31 μm: 98%, <16 μm: 57.5%, <5.5 μm: 3.5%, <2.8 μm: 1.2%
Coarse alumina, Saint Gobain #153PT, (−45 + 15 μm nominal)	Spherical, plasma densified	Al_2O_3 99.6 wt%	α-Al_2O_3, γ-Al_2O_3	<80 μm: 93.75%, <40 μm: 56.27%, <20 μm: 12.69%, <10 μm: 1.12%
Mullite, Saint Gobain #1020 (−45 + 10 μm nominal)	Angular, fused and crushed	Al_2O_3 77 wt.%, SiO_2 22.5 wt.%, Na_2O 0.20 wt.%, Fe_2O_3 0.08 wt.%, others: <0.50 wt.%	Mullite ($3Al_2O_3{\cdot}2SiO_2$)	<80 μm: 99.77%, <40 μm: 84.72%, <20 μm: 31.93%, <10 μm: 5.04%, <1 μm: 1.68%

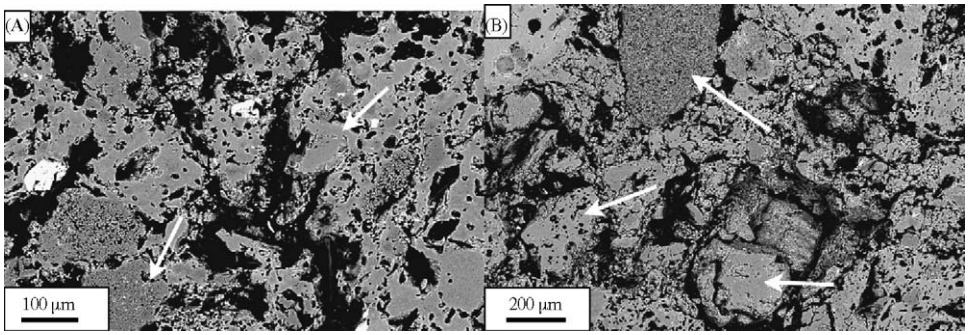

Fig. 2. SEM micrographs of sintered refractories. White arrows indicate some large alumina grains: (A) EXTRA55; (B) EP.

Table 6
Refractory substrates measured properties

	EP	EXTRA55
Porosity (mercury porosimetry)	24%	19%
Porosity (image analysis)	19%	18%
Thermal expansion coefficient ($\times 10^{-6}\,^{\circ}C^{-1}$)	4.85 (200 °C < T < 1200 °C)	5.73 (200 °C < T < 1200 °C)
Normalized wear volume (mm^3/m)	12.7 ± 1.8	4.3 ± 0.5

The measured properties of the substrates are listed in Table 5. Confirming qualitative observations, the porosity determined from mercury porosimetry is around 20% for both substrates, indicating the material has poor sintering due to the low reactivity of these ceramic phases at high temperature. The results from mercury porosimetry and image analysis are quite similar, indicating that image analysis can be considered a reliable porosity evaluation technique for the substrates. As far as the coatings are concerned, the specimen preparation could cause pull-outs, so that the measured porosity value got by image analysis can be higher than the actual one. Nevertheless, this possible overestimation does not interfere with our design of the coatings, because, at most, the final consequence is being more strict in the powder and spraying parameters choice to improve the coating quality.

The thermal expansion coefficients are very important for the interpretation of thermal shock test results. The recorded thermal expansion curves are not completely linear, probably because of distorsive phase transitions which cristobalite undergoes during heating, with significant volume change[26]; the values reported in Table 6 are average values measured between 200 °C (to exclude the initial instrumental drift) and 1200 °C. It can be seen that they are considerably low values when compared to that of plasma-sprayed alumina, which is reported in literature[17] to be about $7.24 \times 10^{-6}\,^{\circ}C^{-1}$; thus, pure alumina cannot be directly sprayed onto the refractory: according to the substrate, a $2.39 \times 10^{-6}\,^{\circ}C^{-1}$ or a $1.51 \times 10^{-6}\,^{\circ}C^{-1}$ difference in thermal expansion coefficients would cause very high thermal expansion mismatch stresses, particularly when cooling the system down from very high temperatures. If the coating plus substrate system is heated up to very high temperatures, close to the upper operating limit of the substrate, some creep relaxation, which limits the compressive stresses arising in the coating and the consequent tensile ones in the substrate, becomes possible, but if the system is then cooled down to low temperature, tensile stresses arise in the coating, which may cause transversal cracking through the coating or delamination at the coating–substrate interface. A very simple finite elements estimate of such stresses, with a software which accurately accounts for the actual coating microstructure, i.e. porosity and thermo-mechanical properties of the different phases,[27] gives an average tensile stress of 90 MPa in the whole coating and of 280 MPa close to the interface when cooling down from 1400 °C to 25 °C, meaning that complete coating fail-

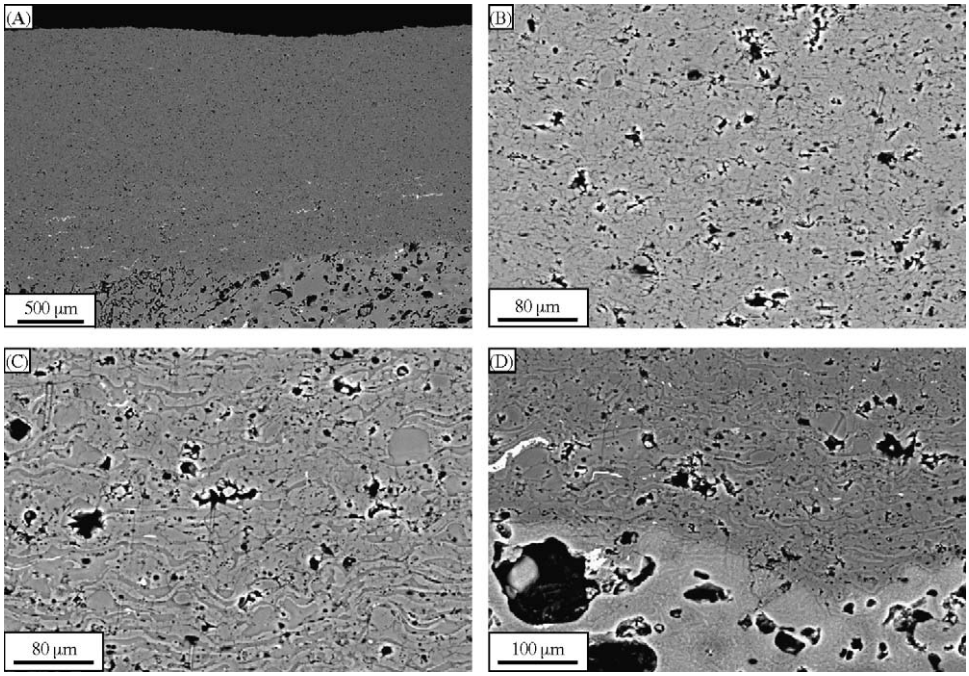

Fig. 3. SEM micrographs of two-layered coating on EXTRA55 substrate, cross-section: (A) general view; (B) alumina layer, detail; (C) 30 vol.% mullite–70 vol.% alumina layer, detail; (D) interface with substrate, detail.

ure would very likely occur. This is the reason why layered systems were employed.

3.2. Microstructure and wear resistance of coatings

Fig. 3A–D shows the microstructure of the as-sprayed two-layered coatings; it can be noticed that the alumina top layer has a low porosity microstructure (Figs. 3B and 4): the porosity determined by image analysis is, in all cases, comparable to some high-quality plasma-sprayed coatings described in literature.[28–30] The lower layer (Fig. 3C) has a slightly more defective microstructure, with higher porosity, which, apart from pull-outs caused during the specimen preparation, may be due both to rounded pores, which are attributable to gas entrapment, and to microcracks, caused by thermal shocking. The larger particle size of the employed powders, non optimal spraying parameters (in particular, for the two-layered coating, an excessively high 50 kW operating power in the plasma torch was employed), and the different in-flight and solidification progress of mullite and alumina might be the causes of such higher porosity. Literature works indicate that mullite splats generally display no or little microcracking, because mullite possesses excellent thermal shock resistance[31]; alumina splats are renown to develop much microcracking upon solidification, because they relax the tensile quenching stresses.[32] These phenomena seem to take place in this case as well. In fact, in the composite layer, the alumina splats display a high microcracks density, while mullite splats are almost crack-free. No cracks along the interfaces between alumina and mullite splats can be noticed, indicating excellent adhesion: this is probably due to their high chemical affinity. The adhesion to the substrate looks very strong as well (Fig. 3A and D); while plasma-sprayed ceramic coatings on metallic substrates only develop mechanical bonding to the substrate surface asperities, in this case some chemical interaction occurs, as it has formerly been reported in literature for similar systems,[12] particularly because the substrate and the coating contain the same phases (alumina and mullite).

SEM micrographs analysis has shown no major microstructural differences between the three- and four-layered coatings with the simpler ones (see porosity values in Fig. 4). The interface between the coating and the substrate still appears to be very strong, as well as the adhesion between alumina and mullite splats and between the different layers. It can be noticed that the mullite layer has a completely different microstructure from the alumina one, with few microcracks, poorly distinguishable splat interfaces and more rounded pores. This is similar to former results.[33]

X-ray diffraction on all of the coatings indicates that alumina mainly appears as the metastable γ-Al_2O_3 phase, with a low amount of α-Al_2O_3, whose presence reflects the existence of unmelted or partially melted particles. The formation of a metastable, lower density cubic (spinel-like) structure instead of the stable hexagonal corundum structure due to extremely rapid splat quenching is a well known phenomenon.[32] In the mullite layer, mullite diffraction peaks and a broad diffraction band (centred around $2\theta = 26^\circ$), characteristic of a glass phase, coexist. The alumina peaks which are detected are due to the 30 vol.% alumina layer, which has been reached in some spots after polishing because of the large waviness of the coating, reflecting the grit-blasted surface waviness. Since molten mullite contains a significant amount of silica, a typical glass forming oxide and considering the extremely high cooling rates of plasma-sprayed splats, the formation of a glassy phase is quite logical. This fact has already been reported in literature,[33] although the used operating parameters are, in this case, much different. In ref. 33 indeed, the mullite coating was completely glassy, and possessed a slightly different microstructure. The crystalline part of this coating might both be due to partial crystallization, or to unmelted particles. The low width of diffraction peaks may support the latter interpretation, but this is not a conclusive evidence. More research is needed on this matter.

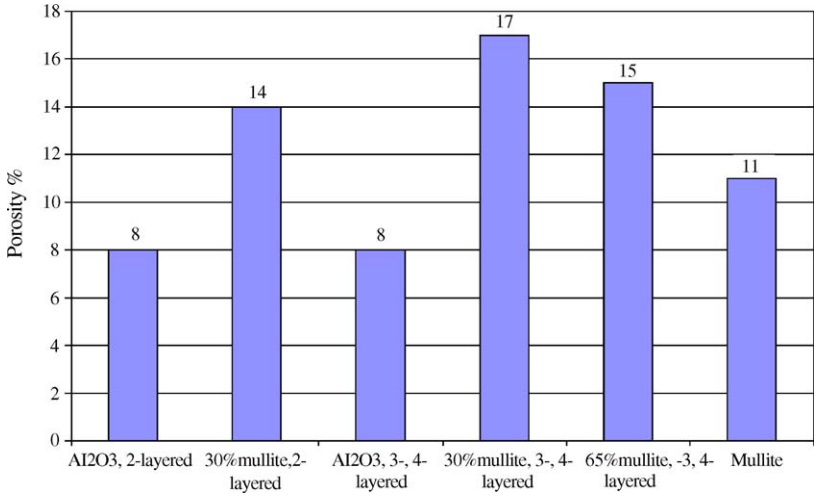

Fig. 4. Porosity of all the layers in as-sprayed two-, three- and four-layered coatings.

The dry particles abrasion resistance of these coatings, which possess a quite dense top layer, exceeds that of the refractory substrates by more than one order of magnitude (wear volume: EP = 12.5 mm^3/m; EXTRA55 = 4.25 mm^3/m; alumina top coating = 0.7 mm^3/m). Indeed, the refractories display very poor wear resistance, even lower than other traditional ceramic materials, whose dry particles abrasion resistance has been tested, under the same experimental

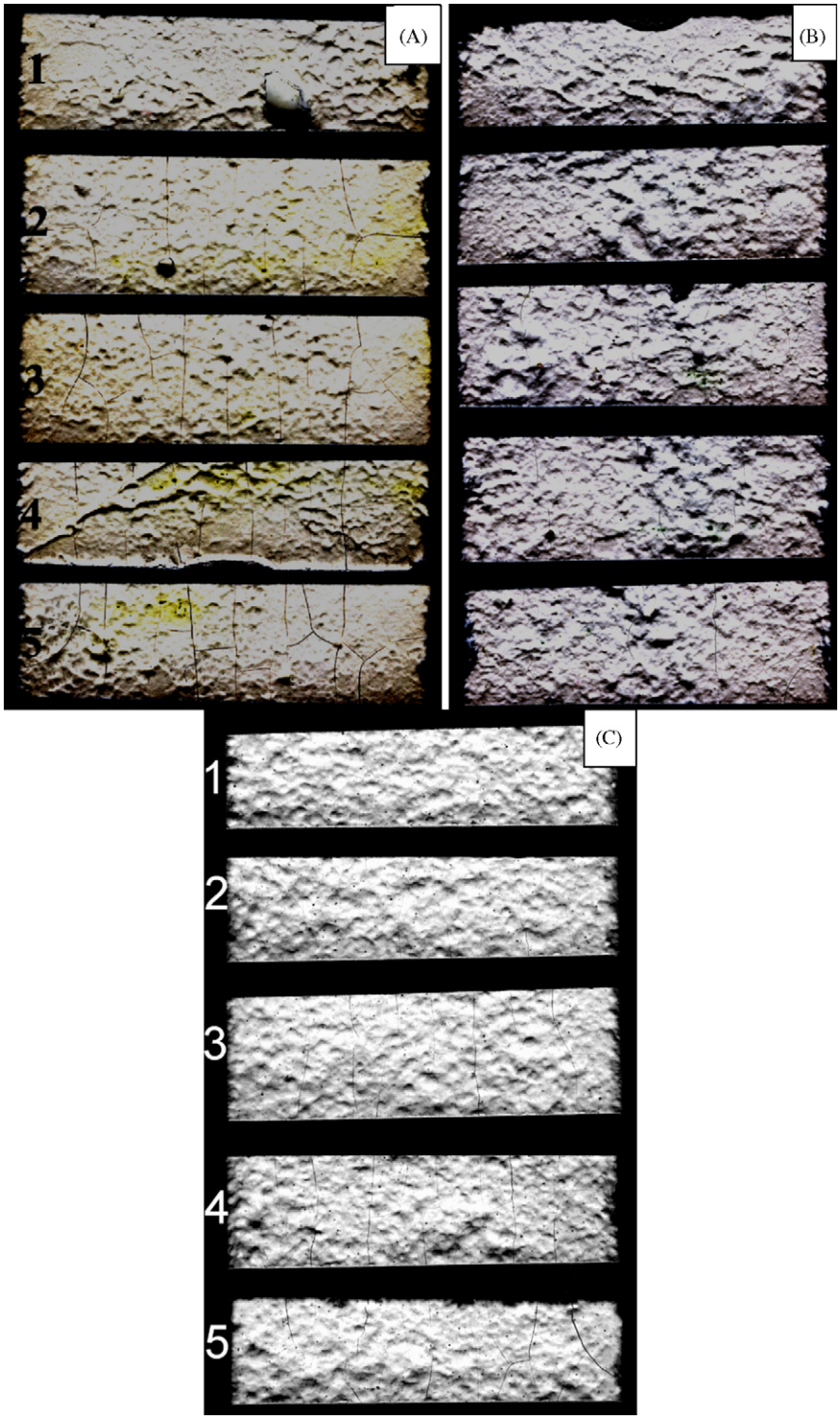

Fig. 5. Digital images of thermally shocked samples. Contrast has been electronically enhanced to highlight the thermal shock cracks. All the samples are 60 mm long and their width varies from 15 to 20 mm: (A) two-layered coating on EXTRA55 substrate; (B) three-layered coating on EXTRA55 substrate; (C) four-layered coating on EP substrate.

conditions.[34] Since all the layered coatings possess the same, thick alumina top layer, no significant differences exist between their performances.

3.3. Thermal shock resistance

Fig. 5A–C is the thermally shocked sample: it can be noticed that, in the two-layered coating (Fig. 5A), no major cracks are present after one cycle, but further cycles cause thermal shock damage. After the second cycle, some cracks are formed; more cracks exist when the samples undergo three cycles; but no more cracks appear in the subsequent cycles. The cracks propagate perpendicularly to the substrate and transversally to the sample longer side; this clearly means that tensile stresses developed in the alumina layer during cooling caused them. Furthermore, cracks in the refractory substrate parallel to the interface exist at the sample ends, they have probably been caused by the high interfacial shear stresses which are developed in these areas. The fact that no coating delamination across the interface took place confirms the strength of the adhesion to the substrate. Microstructural and micromechanical investigation can help highlighting the thermal behaviour. SEM micrographs (Fig. 6A and B) show deep changes in the alumina layer immediately after the first cycle: the splat-like microstructure was lost (compare Fig. 6B to Fig. 3B), rounded grains are visible, together with some microcracks, which are probably due to residual thermal stresses, and porosity significantly increased. As expected,[24] X-ray diffractometry indicates that the coating now mostly consists in α-Al_2O_3, with a very small amount of metastable phases such as δ-Al_2O_3 and θ-Al_2O_3. It can thus be argued that, during heating, enough energy was supplied to the material for the $\gamma \rightarrow \alpha$ phase transition to occur and that a limited degree of sintering along the splat interface could take place. Therefore, the splat-like microstructure disappeared because of sintering, similarly to other studies on high-temperature heat treated plasma-sprayed ceramic coatings[23]; phase transformation, and possibly also crystal grain growth phenomena, resulted in rounded crystal grains. The definitely lower diffraction peaks width in the thermally shocked samples than in the as-sprayed ones indicates that the average grain size has largely increased, confirming a grain growth process by sintering of splats and merging of nearby grains. Since α-Al_2O_3 possesses a higher density than γ-Al_2O_3, the phase transformation causes a shrinkage of the crystals, thus resulting in increased porosity. The fact that the coating did not crack due to this phase change (in fact, no cracks were noticed immediately after the samples were taken out of the kiln after the first shock cycle) can be due to two reasons. On the one hand, since the as-sprayed coating possesses limited cohesion and since sintering and phase transformation occur simultaneously, some of the newly formed crystals were allowed to shrink quite freely before too much sintering occurred. On the other hand, it seems from SEM micrographs that sintering occurred to a greater degree in the direction perpendicular to the substrate, across splat interfaces, whose contact points probably act as pre-existing necks, and to a lesser one in the direction parallel to the substrate, probably because intra-splat microcracks obstacled it. Thus, vertical microcracks remain, allowing crystals shrinkage in the direction parallel to the substrate interface.

In the composite layer, the alumina splats, after one thermal shock cycle, were analogously transformed (Fig. 7), while mullite looks unchanged. The latter behaviour could be explained with the high temperature needed to sinter mullite (>1600 °C).[35]

Thermo-mechanical properties (elastic modulus, thermal expansion coefficient) for plasma-sprayed self-standing alumina and mullite layers are reported in Table 7. The increase in the elastic modulus after the thermal treatment is a consequence of sintering, in accordance with ref. 23, and is certainly unfavourable for thermal shock resistance, because a stiffer material develops higher stresses in the presence of CTE mismatches. The higher elastic modulus increase for alumina (≈23%) than for mullite (≈12%) also confirms the higher degree of sintering occurring for alumina than for mullite. No other major microstructural changes occur in the subsequent cycles, as porosity does not perceivably increase after the first cycle (Fig. 8). The alumina crystallographic transformation after one cycle is complete, leaving α-alumina as only phase. The continuous superposition of residual stresses leads to cracking; thus, the number of macroscopic cracks increases, reaching its maximum after the third cycle. SEM micrographs (Fig. 9) indicate that most of the

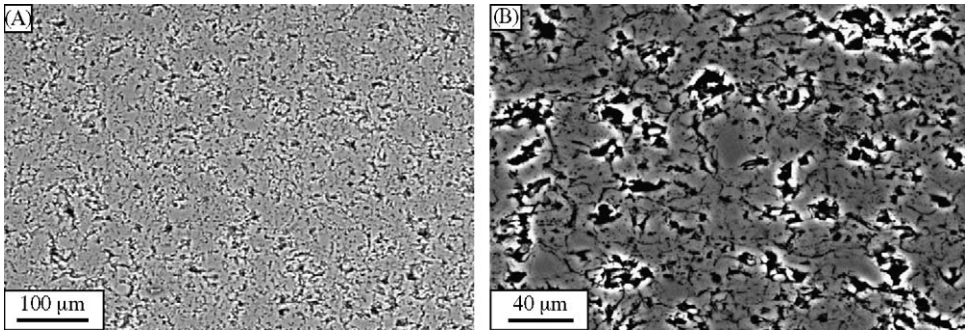

Fig. 6. SEM micrographs of thermally shocked alumina layer in two-layered coating on EXTRA55: (A) cross-sectional view; (B) cross-section, detail.

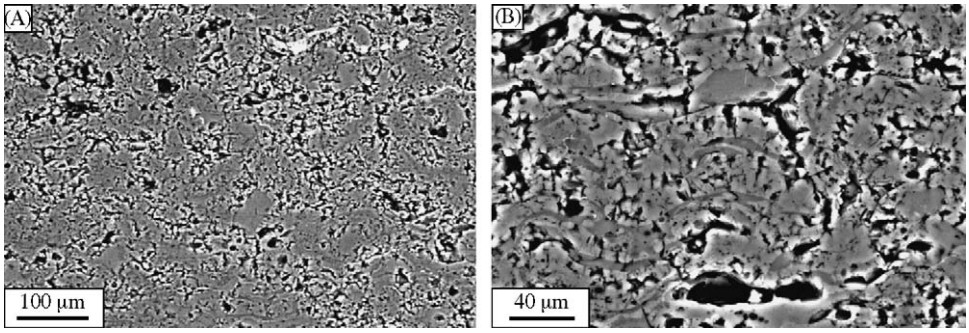

Fig. 7. SEM micrographs of thermally shocked 30 vol.% mullite–70 vol.% alumina layer in two-layered coating on EXTRA55: (A) cross-sectional view; (B) cross-section, details.

Table 7
Thermo-mechanical properties of self-standing plasma-sprayed alumina and mullite

	E (GPa), before heat treatment	E (GPa), after heat treatment	α (°C^{-1}), 100–1000 °C after heat treatment
Al_2O_3	215.73 ± 15.07	264.39 ± 41.67	7.69×10^{-6}
Mullite	147.25 ± 19.61	164.22 ± 33.33	4.93×10^{-6}

cracks start at the coating surface and propagate vertically across the coating, down to the substrate, but cause no interfacial delamination. Instead, cracks parallel to the interface are sometimes present in the refractory, like the one shown in Fig. 9. Transverse cracks are probably due to the high tensile stresses which develop in the alumina layer both because of its high thermal expansion coefficient and of temperature gradients occurring during cooling, due to the insulating nature of these materials. These latter non-steady-state effects cause an additional tensile stress in the top layer. The longitudinal cracks in the substrate are probably due to the shear stresses which arise around the interface because of thermal expansion coefficients mismatch; the fact that cracking never occurs at the interface but inside the substrate itself confirms the excellent adhesion strength.

The three-layered coatings (Fig. 5B) appear to possess an improved thermal shock resistance; in fact, almost no cracks appear even after two cycles, few are present after three cycles, and no more are formed in the following cycles.

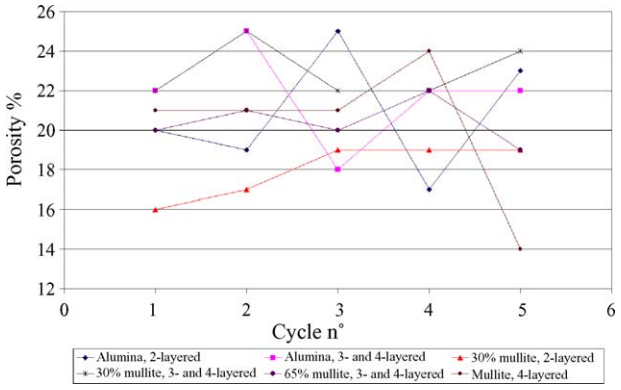

Fig. 8. Porosity of all the layers in thermally shocked two-, three- and four-layered coatings.

Furthermore, cracks in the refractory parallel to the interface are absent or definitely smaller. This clearly indicates that the more gradual transition between the thermal expansion coefficient of the substrate and the alumina top coating lessens all the thermal stresses. From SEM micrographs (Fig. 10A–C for three-layered coating; Fig. 11 for mullite layer in four-layered coating: other layers are analogous to the former ones) and X-ray diffraction, it appears that the alumina top layer still undergoes the same phase transformation with porosity increase (Fig. 8), while, in the underlying layers, mullite does not undergo major microstructural changes. Thermal shock microcracks are still visible in the composite layers, and still it seems that they are mainly initiated inside the alumina splats (Fig. 12). SEM micrographs of thermal shock macrocracks (Fig. 13A–C) highlight a very interesting phenomenon: cracks do not propagate straightforwardly across the coating, as it happened in the former case, but

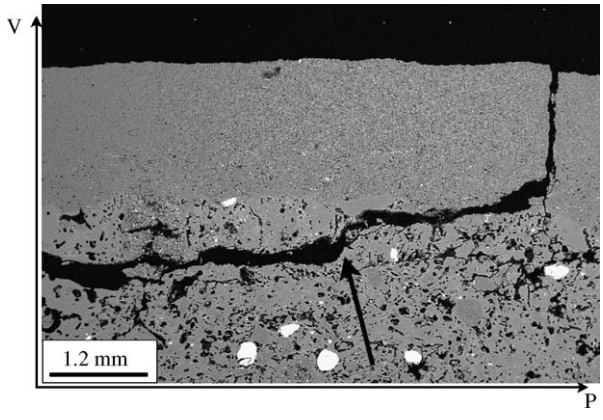

Fig. 9. SEM micrograph of a thermal shock crack in the two-layered coating on EXTRA55 substrate after four cycles. Black arrow marks the crack parallel to the interface in the substrate. V and P axes indicate the vertical direction and the direction parallel to the substrate, respectively.

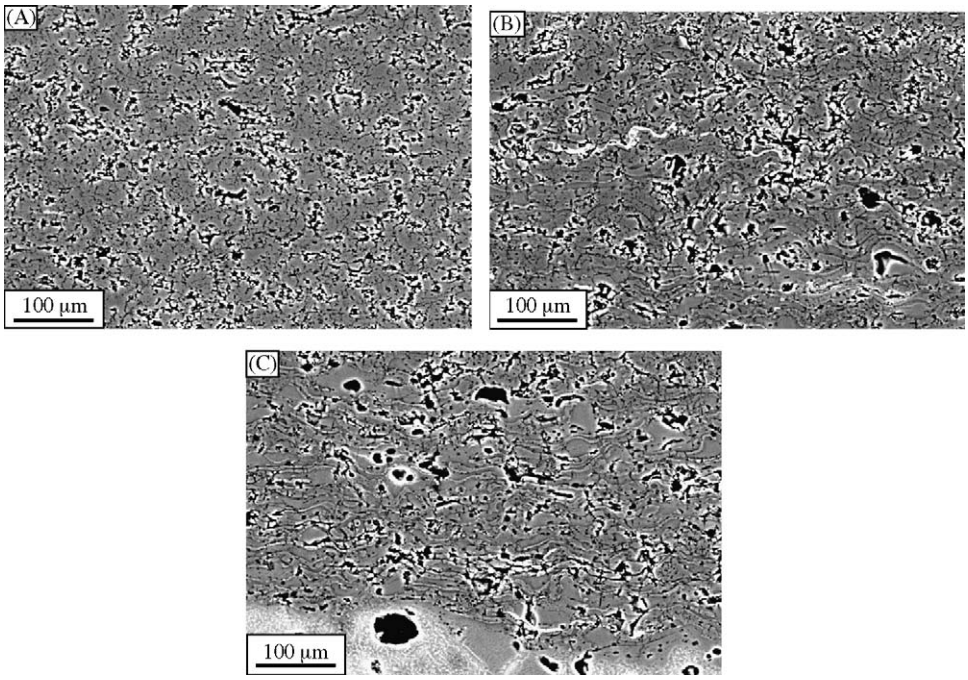

Fig. 10. SEM micrographs of thermally shocked three-layered coatings, cross-section: (A) alumina layer; (B) 30 vol.% mullite–70 vol.% alumina layer; (C) 65 vol.% mullite–35 vol.% alumina layer.

are often deflected upon reaching the lower layers, where they propagate parallel to the substrate (see black arrows in Fig. 13A). They seem to propagate across the 65 vol.% mullite layer or across the interface with the 30 vol.% mullite layer, and detailed micrographs indicate they mainly cross alumina splats (see black arrows in Fig. 13B), confirming the former observations concerning the higher alumina tendency to thermal shock cracking. The fact that, even when microcracks are formed, they do not propagate down to the substrate but are deflected is very promising for combined thermal and chemical resistance, because, if a transverse crack directly leading to the substrate was formed, a corrosive media could easily reach the substrate itself.

Four-layered coatings on EP substrates, unfortunately, do not show the same thermal shock resistance improvement: Fig. 5C, in fact, highlights that a significant amount of cracks appear within the first three cycles, as it happened in two-layered ones. SEM micrographs, however, still indicate that cracks are often deflected parallel to the substrate; this happens upon reaching the interface between the 65 vol.% mullite layer and pure mullite layer (Fig. 13C, see black arrow).

The thermal shock behaviour can now be interpreted on the basis of the measured thermo-mechanical properties. First of all, the different thermal shock behaviour of alumina and mullite splats (with the latter looking more resistant) must be explained. In literature, formulae like the following are

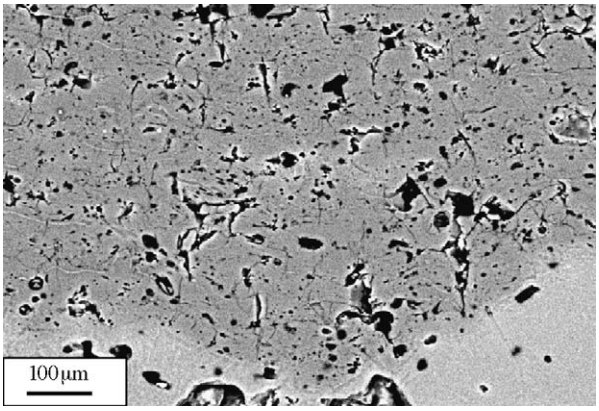

Fig. 11. Thermally shocked mullite layer in four-layered coating. The other thermally shocked layers in four-layered coatings are analogous to the ones in Fig. 14.

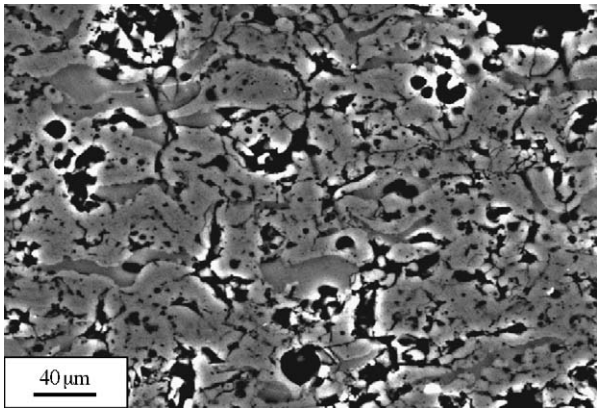

Fig. 12. SEM micrograph of 65 vol.% mullite–30 vol.% alumina layer in three-layered coating on EXTRA55 substrate after two thermal shock cycles, detail of cross-section.

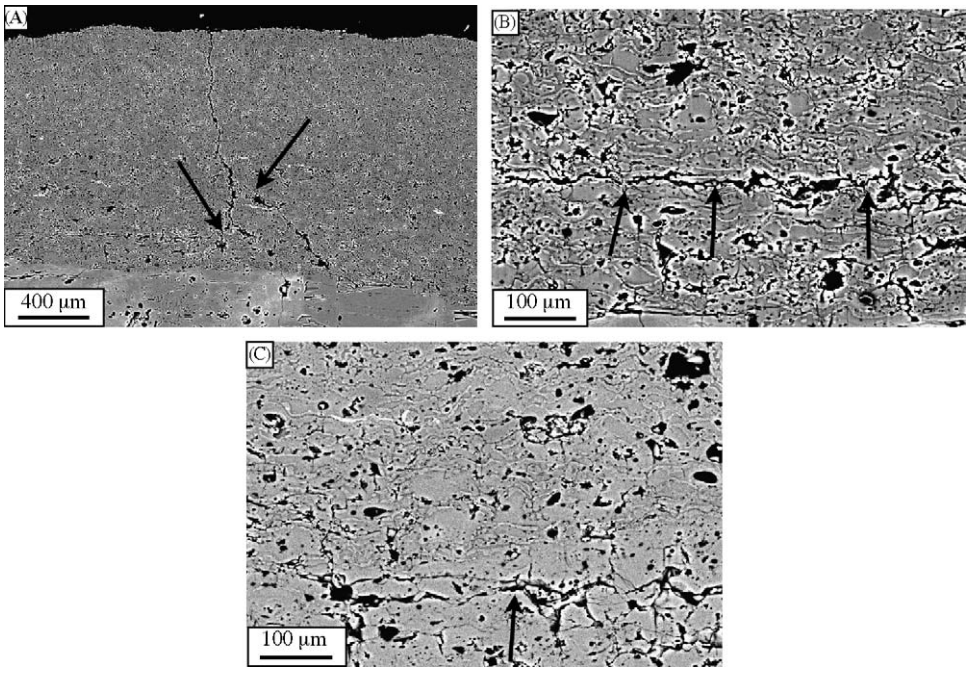

Fig. 13. SEM micrographs of thermal shock cracks in 3- and four-layered coatings. (A) Deflected crack in three-layered coating after three cycles (black arrows highlight deflection). (B) Detail of deflected crack running parallel to the substrate across the 65 vol.% mullite layer in three-layered coating after three cycles (The black arrow highlights the crack propagation mostly across alumina splats.) (C) Detail of deflected crack running parallel to the substrate near the interface between mullite layer and 65 vol.% mullite layer in four-layered coating after three cycles (black arrow highlights the crack running in the mullite layer, close to the layers interface).

reported for thermal shock resistance evaluation[36]:

$$R = \frac{\sigma_f(1-\nu)}{E\alpha}\kappa \quad (2)$$

where R = parameter predicting the thermal shock resistance, expressing the conditions for failure by crack initiation (W/m); σ_f = tensile strength (MPa); ν = Poisson's ratio; E = elastic modulus (MPa); α = thermal expansion coefficient ($^\circ C^{-1}$); κ = thermal conductivity (W/m °C).

Employing the measured values of E and α for thermally sprayed alumina and mullite, as well as literature values for κ and σ_f, it follows:

alumina: $E = 264.39 \times 10^3$ MPa, σ_f (ref. 17) = 10 MPa, $\nu = 0.23$, $\alpha = 7.69 \times 10^{-6}\,^\circ C^{-1}$, κ (ref. 17) = 25.2 W/(m °C) $\Rightarrow$ $R = 95.44$ W/m; mullite: $E = 164.22 \times 10^3$ MPa, σ_f (ref. 33) = 91 MPa, $\nu = 0.23$, $\alpha = 4.93 \times 10^{-6}\,^\circ C^{-1}$, κ (ref. 37) = 1.32 W/(m °C) $\Rightarrow$ $R = 114.24$ W/m.

Thus, mullite is predicted to possess a better thermal shock resistance, explaining its lower tendency to thermal shock cracking and the preferential thermal shock cracks propagation across plasma-sprayed alumina splats.

The crack propagation behaviour across layers must now be interpreted in the light of thermal expansion coefficient of the various layers. With Eq. (1), the thermal expansion coefficient of all the layers are computed and collected in Table 8, while the thermal expansion coefficients mismatches between adjacent layers and between layers and substrate are listed in Table 9. It is immediately apparent that, in the two-layered coatings, the greater mismatch is between the bottom layer (30 vol.% mullite) and the substrate. This causes high interfacial shear stresses, accounting for the substrate cracks parallel to the interface; in fact, the weakest part of this system seems to be the substrate itself. In the three- and four-layered coatings, the bottom layer-substrate CTE mismatch is very small. In the three-layered the greater mismatch lies between

Table 8
Thermal expansion coefficients of all layers and of substrates

Layer	α ($\times 10^{-6}\,^\circ C^{-1}$)
100% Alumina	7.69
30% Mullite–70% alumina	7.11
65% Mullite–35% alumina	6.21
100% Mullite	4.93
Substrate: EXTRA55	5.73
Substrate: EP	4.85

Note: CTEs of composite layers were calculated with Eq. (1).

Table 9
Thermal expansion coefficient mismatches between adjacent layers

Layers	$\Delta\alpha$ ($\times 10^{-6}\,^\circ C^{-1}$)
Alumina–30% mullite	0.58
30% Mullite–65% mullite	0.90
65% Mullite–100% mullite	1.28
100% Mullite–EP substrate	0.08
30% Mullite–EXTRA55 substrate	1.38
30% Mullite–EP substrate	2.26
65% Mullite–EXTRA55 substrate	0.48

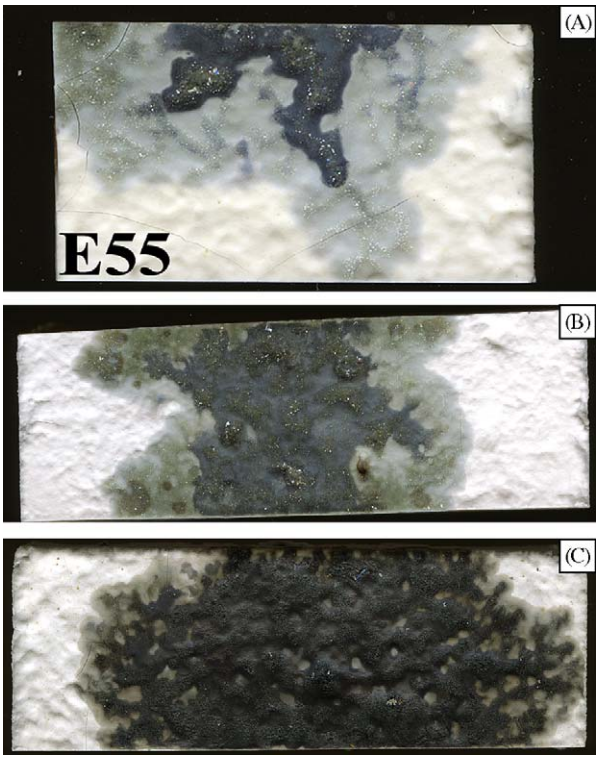

Fig. 14. Digital images of chemically tested samples (the glass has a dark blue colour because of the high content of NiO, CoO, MnO_2): (A) two-layered coating on EXTRA55 substrate (1400 °C test temperature); (B) three-layered coating on EXTRA55 substrate (1400 °C test temperature); (C) four-layered coating on EP substrate (1300 °C test temperature).

the 30 vol.% mullite layer and the 65 vol.% mullite layer; in the four-layered, it lies between the 65 vol.% mullite layer and the pure mullite one; thus, the greater shear stresses are located at these interfaces. This perfectly matches the experimental observations showing cracks shifting from perpendicular to parallel to the substrate interface exactly along these layer boundaries. Obviously, these results point out to the fact that future developments must include an improved layered structure design to decrease and equally part the CTE mismatch among layers.

3.4. Chemical resistance

Fig. 14A–C shows the two-, three- and four-layered coated samples after the chemical resistance test. Fig. 15A and B is the cross-sectional SEM micrograph of the chemically tested uncoated refractories: it is obvious that they underwent a deep glass penetration, with depths of more than half millimetre to 2 mm. The glass infiltrated the numerous open pores and dissolved the phases with lower chemical resistance, like mullite; consequently, the alumina grains float unsupported in the glass (see black arrows), undergo increasing chemical attack, and are dragged away by convection motions inside the glass itself. Eventually, the refractory would disrupt. X-ray diffractometry confirmed that corundum is the only crystalline phase on the surface of corroded refractories, confirming that the mullite phase which bonded the alumina grains was easily removed by the glass percolating into the pores.

In all the tested coatings, instead, SEM micrographs (Fig. 16A–E for two-layered coatings on EP and EXTRA55, Fig. 18 for three-layered coatings on EXTRA55 and four-layered coatings on EP) indicate that the coatings have been very little affected by the molten glass, and fundamentally retained their original structure (Fig. 16A). Detailed SEM micrographs indicate that significant alterations were caused by glass penetration just down to a depth of about 50 μm (Fig. 16B and C). In such very thin layer, alumina reacted with the glass: it was probably partially dissolved and then re-crystallized due to glass saturation, so that large polygonal alumina grains appear. On top of that re-crystallized layer, several small polygonal crystals are present, looking very bright in backscattered SEM micrographs. According to EDS microanalysis, they contain large amounts of Al and Ni and smaller amounts of Co, Mn, Fe, Zn. X-ray diffraction reveals that these grains are Ni-based spinel ($NiAl_2O_4$), containing other metal ions in solid solution: presumably, they are the result of some chemical reaction between the glass and the dissolved alumina. Superficial SEM micrographs confirm that the glass reacted with alumina on the very surface, causing re-crystallization; such re-crystallization sometimes produces peculiar microstructures, like extremely smooth,

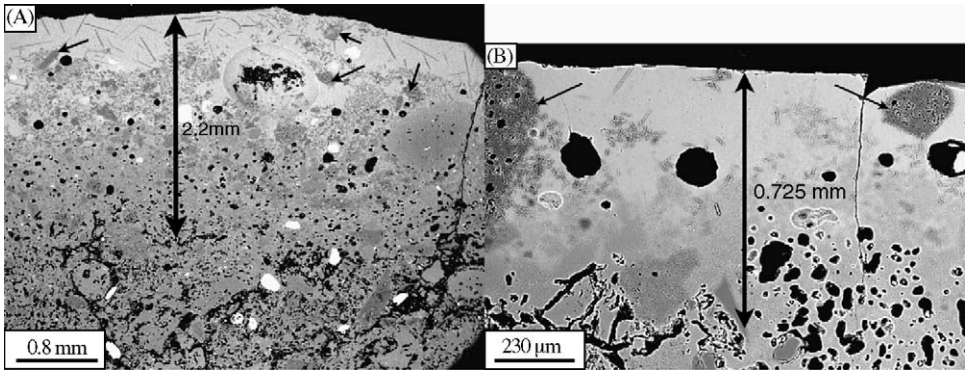

Fig. 15. SEM micrographs of chemically tested uncoated refractories, cross-sections: (A) EXTRA55, 1400 °C test temperature; (B) EP, 1300 °C test temperature. Black arrows indicate unsupported alumina grains floating in the glass.

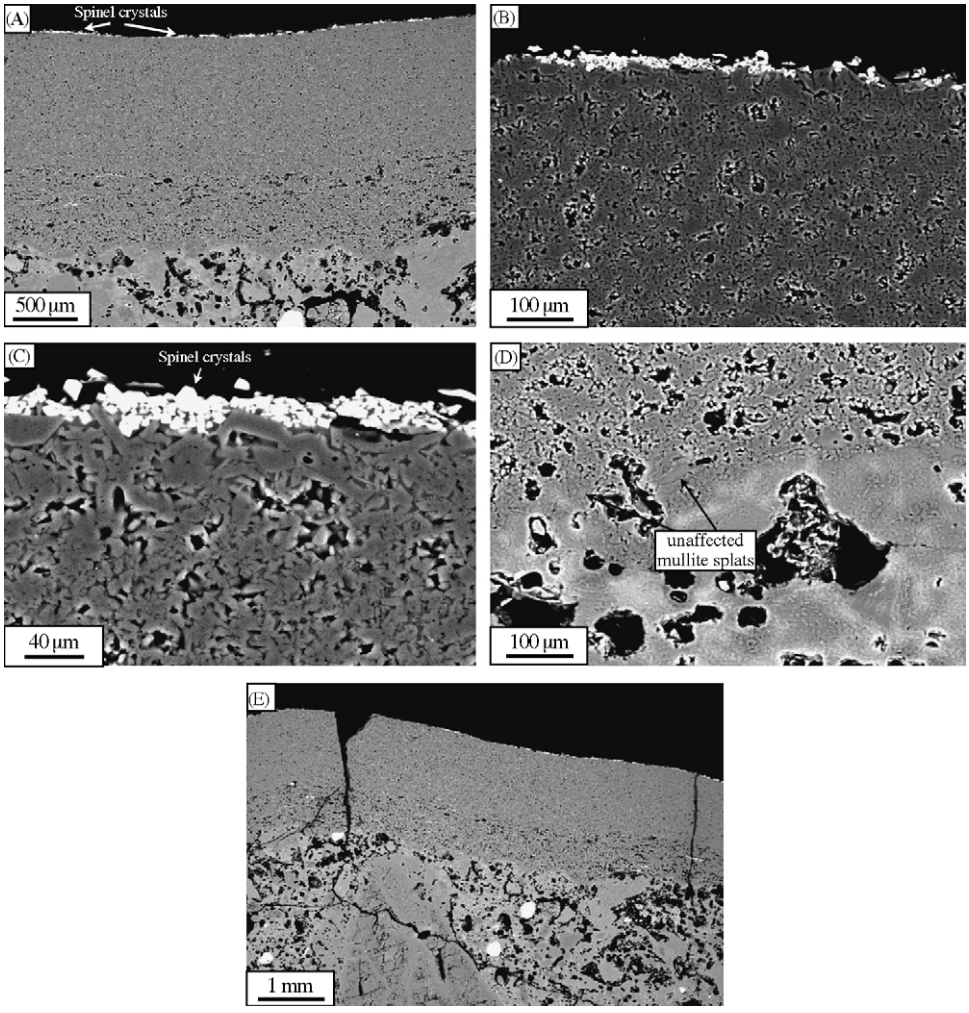

Fig. 16. SEM micrographs of chemically tested two-layered coating on EXTRA55, cross-section: (A) general view; (B) alumina layer; (C) alumina layer, detail near the surface; (D) 30 vol.% mullite layer with substrate interface; (E) general view with thermal shock cracks.

lamellar grains (Fig. 17A) or larger, blocky grains where the growing crystal planes are recognizable (Fig. 17B). Below the thin surface re-crystallized area, most of the alumina layer retained its unaltered microstructure (Fig. 16C). From EDS analysis, a small amount of SiO_2–CaO glass (depleted in the transitional metal ions because of the surface reaction) infiltrating the pores is detectable. This results in a porosity reduction of the top alumina layer down to about 4–5%. Therefore, this limited amount of infiltrated glass does not impair the coating performance; instead, it acts as a

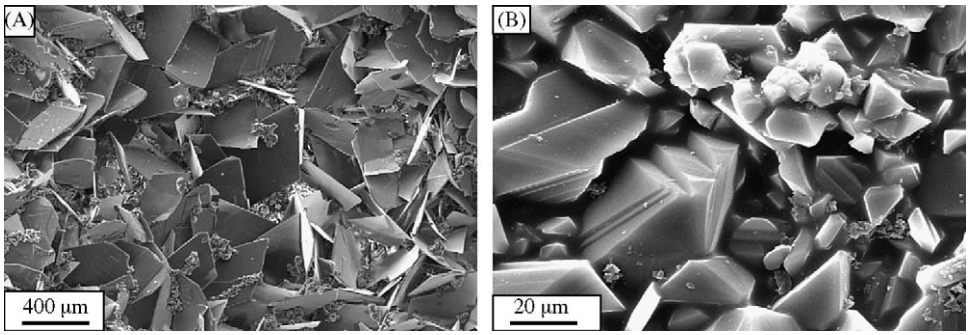

Fig. 17. SEM surface view of chemically tested coatings: (A) extremely thin lamellar alumina crystals, with very small spinel grains among them; (B) polygonal alumina grains, with crystal growth planes clearly visible.

top layer sealant, hindering further glass percolation. On the other hand, the presence of the glass is detrimental to thermal shock resistance both in itself and because it nullifies the advantage of the low modulus as-sprayed microstructure. In the two-layered coating, the lower composite layer was partly affected by some of the percolating glass, which reacted with mullite splats, altering their appearance: some Ca, an element which is present in the glass but not in the plasma-sprayed layers, is detectable by EDS in the altered mullite splats (Fig. 16D). However, the composite layer was not excessively attacked; in fact, it retained its fundamental microstructure, and completely prevented the glass from reaching the substrate: unaltered mullite splats exist next to the substrate interface (Fig. 16D). The mullite alteration by the molten glass confirms its low chemical resistance, which has already been highlighted by the heavy glass attack on the substrate. As the thermal shock tests indicated, transverse cracks appeared during cooling (Fig. 16E); these cracks would be preferential paths for glass penetration to the substrate if the refractory was to undergo a second operating cycle.

The three-layered coating has a very similar appearance; the glass altered the first 50 μm of the top alumina layer (Fig. 18A) and partially infiltrated the small pores (Fig. 18B and C), reducing its overall porosity. In both cases, the glass never attacked the lower layers; in fact, only in the 30 vol.% mullite layer displays some limited evidence of molten glass alteration, while mullite seems absolutely unaltered both in the 65 vol.% mullite layer and the pure mullite one. Microcraks are much less numerous and, as already observed in the thermal shock tests, they do not reach down to the substrate, but are deflected parallel to the substrate across the 65 vol.%

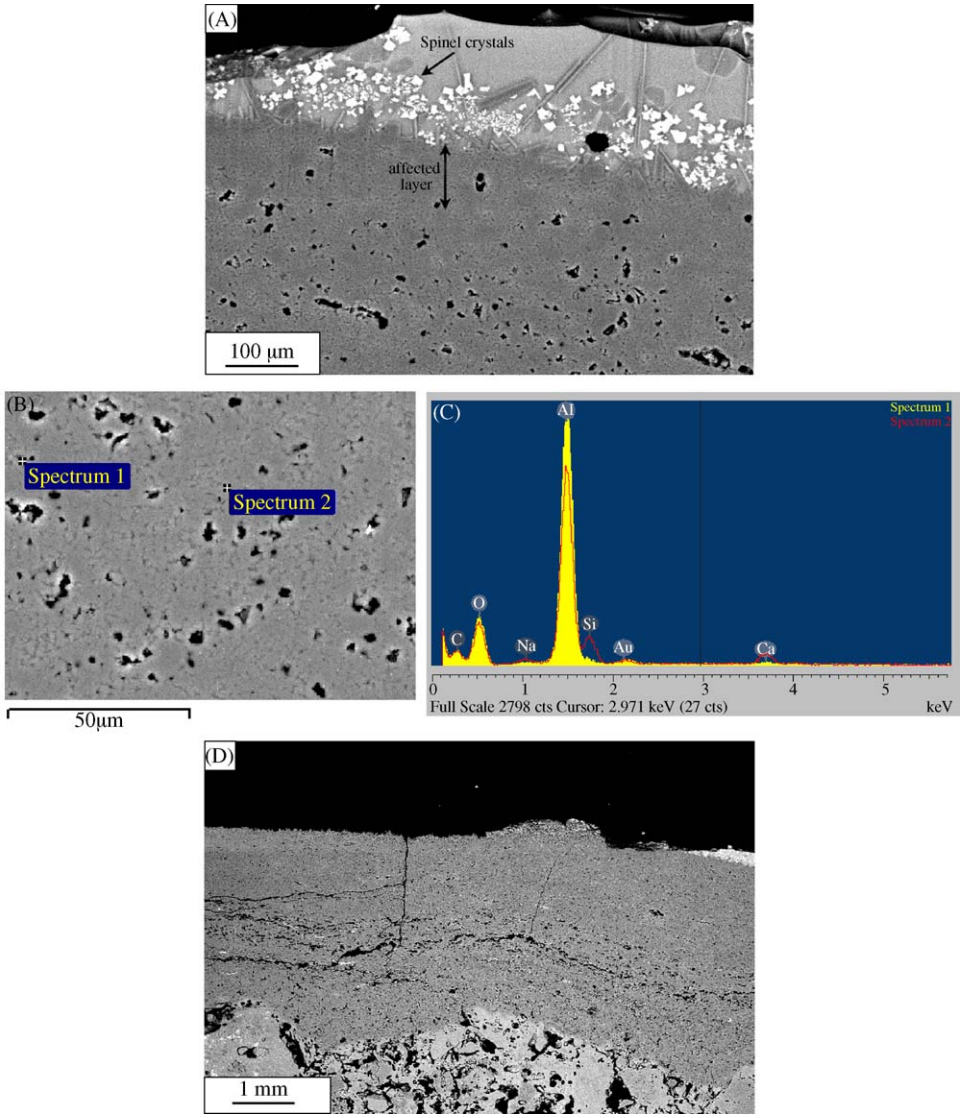

Fig. 18. SEM micrographs of chemically tested 3- and four-layered coatings, cross-sections: (A) alumina layer near the surface; (B) alumina layer under the surface; spectrum 1 and 2 label the two microanalysis spots made on it; (C) EDS spectra, the presence of Si, Ca and Na in spectrum 2 indicates percolated glass from the surface; (D) deflected cracks in four-layered coating on EP substrate.

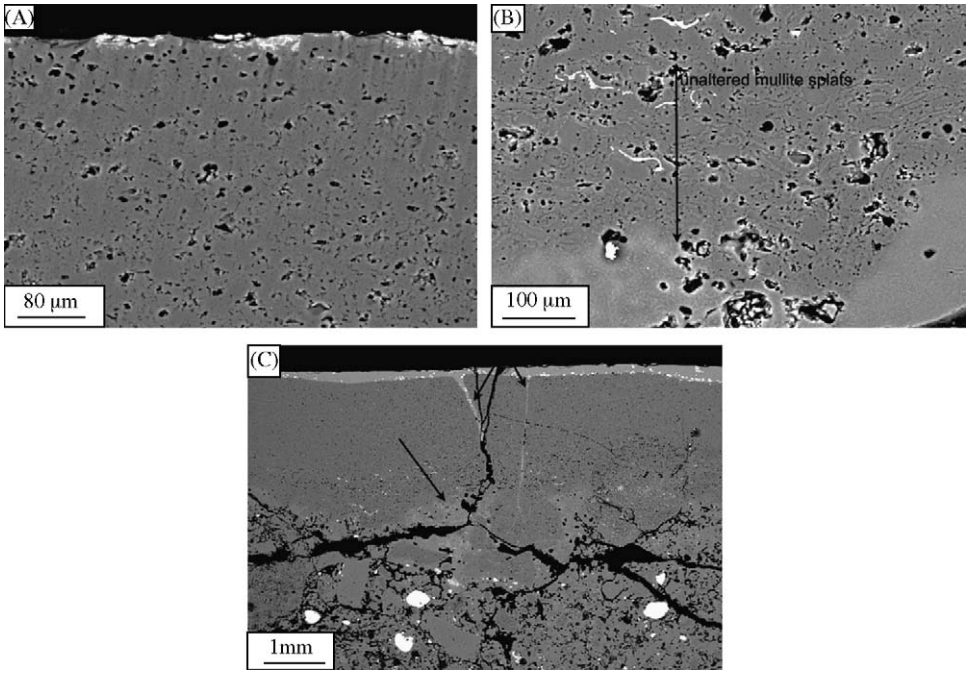

Fig. 19. Cross-sectional SEM micrographs of thermo-chemically tested two-layered coatings: (A) alumina layer near the surface after four cycles; (B) 30 vol.% mullite layer with substrate interface after four cycles, showing unaffected mullite splats for a >100 μm thickness; (C) general view after four cycles with glass percolating down pre-existing cracks and reaching the substrate. Black arrows indicate the glass percolation path and the substrate area reached by the glass.

mullite layer (Fig. 18D). Therefore, in a second operating cycle, the glass would not percolate to the substrate.

3.5. Thermo-chemical cycles

In the two-layered coating, an increasing number of transverse cracks appear during the repeated cycles. The top layer again shows excellent chemical resistance, with pores sealed by molten $CaO–SiO_2$ glass after three cycles (Fig. 19A), as indicated both by the decreasing top layer porosity (Fig. 20) and by the thickness of the unaltered alumina–mullite layer, decreasing in the first three cycles down to a constant value of at least 100 μm from the third to the fifth cycle in all cases (Fig. 19B). However, after some cycles, the transverse

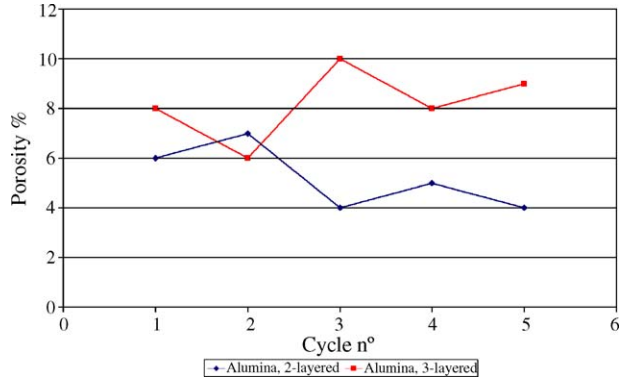

Fig. 20. Porosity of alumina top layer after thermo-chemical cycling tests in 2- and three-layered coatings on EXTRA55 substrate.

thermal shock cracks allow the glass to percolate down to the substrate, as expected, as very clearly noticeable in SEM micrographs (Fig. 19C).

In the three-layered coating, almost no macrocracks were formed after the first cycle, and few are present after the following ones; however, the coating starts undergoing bulging. In the first cycles, some cracks appear in the coating, but, similarly to the thermal shock tests, they are deflected and propagate parallel to the substrate across the 30 vol.% mullite layer. Thus, the molten glass cannot directly reach the substrate in the subsequent cycles (as in two-layered coatings), but large amounts can enter in contact with mullite in some spots: mullite (whose poor chemical resistance, is clearly confirmed also in this case by SEM micrographs) is then dissolved by molten glass, compromising the composite layers cohesion and affecting their mechanical strength. Eventually, in such areas, the alumina splats float unsupported in the molten glass. Thus, bulges are formed by expansion of air entrapped in the pores. After five cycles, the composite layers have been so degraded that the glass has managed to make its way down to the substrate (Fig. 21). Therefore, even though the three-layered coating possesses an enhanced thermal shock resistance, the deflected cracks act detrimentally, rather than beneficially, to the thermo-chemical behaviour after a significant number of cycles, because they constitute easy paths for the molten glass to massively reach the mullite layer, thus thwarting the protective action of the top alumina layer, which would still be effective, as the 65 vol.% mullite layer remains unaltered in those areas where the glass could not penetrate through the deflected cracks.

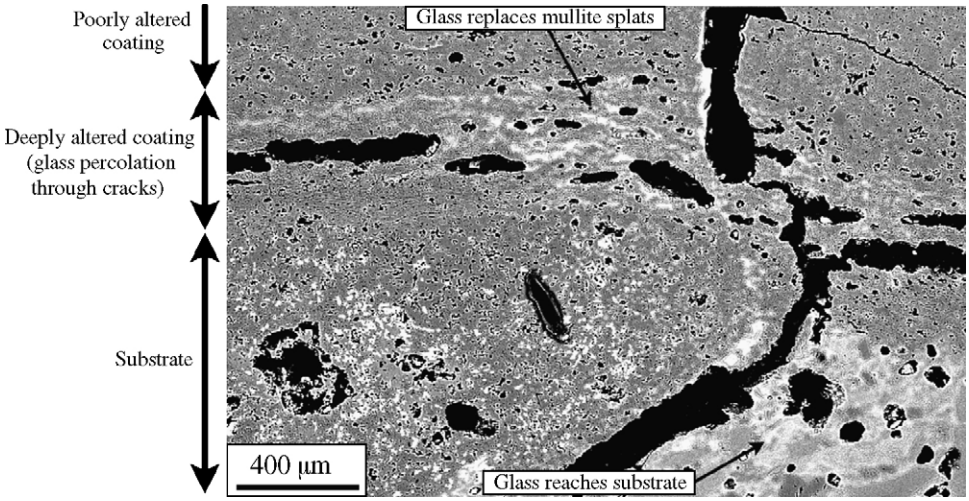

Fig. 21. Cross-sectional SEM micrograph of three-layered coating after five thermo-chemical cycles showing that the glass percolated through the deflected cracks has dissolved the mullite splats, disrupted the 65 vol.% mullite layer and made its way down to the substrate.

4. Conclusions

In the present work, thick corrosion resistant ceramic coatings have been plasma-sprayed on sintered ceramic refractories, aiming at a substantial improvement of the wear and corrosion resistance of the substrates, so that they can be employed in very aggressive industrial environments, for instance in molten glass processing plants.

The following conclusion can be drawn from Section 3:

- 1 mm thick protective layered coatings on sintered alumina–mullite low cost refractories, with a thick ($\geq$400 μm), low porosity ($\approx$6%) alumina top layer and alumina–mullite composite lower layers were successfully produced by plasma-spraying pure ceramic powders with a double feeding equipment.
- The coating adhesion to the substrate was found to be excellent; in fact, in no cases coating delamination at the interface did occur after thermal or chemical tests.
- The coating improves by almost one order of magnitude the abrasion resistance with respect to the uncoated refractory substrate.
- The chemical resistance to continuous contact with molten glass was also largely enhanced: the sintered refractory uncoated surface is disrupted by the glass, which penetrates down to 1–2 mm into the material, easily dissolves mullite and other low chemical resistance phases, and removes alumina blocks by convective motions; the coating, instead, undergoes no significant structural changes (with an altered surface layer of barely $\approx$50 μm) and completely prevents the molten glass from reaching the substrate.
- However, a two-layered coating has poor thermal shock resistance, because thermal stresses accumulate during cooling. Cracks in the coating, perpendicular to the interface, are formed due to tensile stresses; cracks in the substrate, parallel to the interface, are formed by tangential stresses around the interface. The CTE mismatch between bottom layer and substrate was found to be too high. Under combined thermal and chemical cycling, the top layer offered a very effective barrier against the molten glass, with the small pores being sealed by the glass and eventually preventing any further glass penetration after three cycles; however, the transverse cracks allowed some glass to reach the substrate in certain locations after some cycles.
- Three-layered coatings on EXTRA55 substrate possess improved thermal shock resistance, as cracks are much less numerous and deflected from perpendicular to parallel to the interface, but layers design should be improved in order to achieve an equal partitioning of the CTE mismatch between layers. The excellent chemical resistance has not been impaired. Unfortunately, four-layered coatings on EP substrate still develop a great number of thermal shock cracks, although the cracks are again deflected. Again, the layered structure must be improved to avoid large CTE differences between some adjacent layers. Under combined thermal and chemical cycling, the three-layered coating is bulged, because the deflected cracks allow the glass to reach the composite layers and dissolve the mullite splats, compromising their mechanical strength; eventually, the glass can reach the substrate by dissolving more and more mullite splats.
- Therefore, future developments involve improving the layered structure of the coating in order to overcome the thermal shock cracking troubles and also testing different materials with good thermo-chemical stability and improved chemical resistance.
- A deeper understanding of the mechanisms leading to thermal shock cracking is also required; therefore, numerical

finite elements simulations are being performed on the coatings with thermo-elastic models in order to reproduce stress distribution and crack propagation paths during cooling. The results of this study will be the subject of a further paper.

Acknowledgements

The authors are grateful to Centro Sviluppo Materiali S.p.A. (Rome, Italy), and in particular to Ing. Fabrizio Casadei, Mr. Edoardo Severini and Mr. Valerio Ferretti, for the plasma-sprayed coatings deposition. We are also very grateful to Delta Refrattari S.p.A. (Capriano del Colle, BS, Italy), and in particular to Mr. Sergio Baruzzi, for supplying the refractory substrates and for their assistance with technical information. The authors wish to thank Dr. Mariano Paganelli and Ing. Chiara Venturelli (Expert System Solutions) for the CTE measurements and suggestions for the analysis of the data.

References

1. Zhu, D. and Miller, R. A., Thermal-barrier coatings for advanced gas turbine engines. In *Thermal-Spray Processing of Materials*, ed. S. Sampath and R. McCune. MRS Bulletin, MRS, Warrendale, July 2000, pp. 43–47.
2. Dorfman, M. R., Thermal spray applications. *Adv. Mater. Processes*, 2002, **160**(10), 66–68.
3. Zhu, D., Nesbitt, J. A., Barrett, C. A., McCue, T. R. and Miller, R. A., Furnace cyclic oxidation behavior of low conductivity thermal barrier coatings. *J. Therm. Spray Technol.*, 2004, **13**, 84–92.
4. Dorfman, M. R., Thermal spray basics. *Adv. Mater. Processes*, 2002, **160**(7), 47–50.
5. Heimann, R. B., Applications of plasma-sprayed ceramic coatings. *Key Eng. Mater.*, 1996, **122–124**, 399–442.
6. Dorfman, M. R., Thermal spray materials. *Adv. Mater. Processes*, 2002, **160**(8), 49–51.
7. Herman, H., Sampath, S. and McCune, R., Thermal spray: current status and future trends. In *Thermal-Spray Processing of Materials*, ed. S. Sampath and R. McCune. MRS Bulletin, MRS, Warrendale, July 2000, pp. 17–25.
8. Celik, E. and Sarikaya, O., The effect on residual stresses of porosity in plasma-sprayed MgO–ZrO_2 coatings for an internal combustion diesel engine. *Mater. Sci. Eng. A*, 2004, **379**, 11–16.
9. Ahmaniemi, S., Tuominen, J., Vuoristo, P. and Mantyla, T., Sealing procedures for thick thermal barrier coatings. *J. Therm. Spray Technol.*, 2002, **11**, 320–332.
10. Uusitalo, M. A., Vuoristo, P. M. J. and Mantyla, T. A., High temperature corrosion of coatings and boiler steels below chlorine-containing salt deposits. *Corros. Sci.*, 2004, **46**, 1311–1331.
11. Li, J. F., Li, L. and Stott, F. H., Multi-layered surface coatings of refractory ceramics prepared by combined laser and flame spraying. *Surf. Coat. Technol.*, 2004, **180–181**, 500–505.
12. Jorge Lino, F., Duarte, T. P. and Maia, R., Development of coated ceramic components for the aluminum industry. *J. Therm. Spray Technol.*, 2003, **12**, 250–257.
13. *Handbook of Thermal Spray Technology*, ed. J.R. Davies and Associates. ASM International, Materials Park, OH, pp. 191–192.
14. Ono, T., *Refractories Handbook*. The Technical Association of Refractories, Tokyo, Japan, 1998, pp. 446–455.
15. Xiong, H. P., Kawasaki, A., Kang, Y. S. and Watanabe, R., Experimental study on heat insulation performance of functionally graded metal/ceramic coatings and their fracture behavior at high surface temperatures. *Surf. Coat. Technol.*, 2005, **184**, 203–214.
16. Widjaja, S., Limarga, A. M. and Yip, T. H., Oxidation behavior of a plasma-sprayed functionally graded ZrO_2/Al_2O_3 thermal barrier coating. *Mater. Lett.*, 2002, **57**, 628–634.
17. Widjaja, S., Limarga, A. M. and Yip, T. H., Modeling of residual stresses in a plasma-sprayed zirconia/alumina functionally-graded thermal Barrier Coating. *Thin Solid Films*, 2003, **434**, 216–227.
18. Khor, K. A. and Gu, Y. W., Thermal properties of plasma-sprayed functionally graded thermal barrier coatings. *Thin Solid Films*, 2000, **372**, 104–113.
19. Gan, Z. and Ng, H. W., Experiments and inelastic finite elements analyses of plasma sprayed graded coatings under cyclic thermal shock. *Mater. Sci. Eng. A*, 2004, **385**, 314–324.
20. Bolelli, G., Cannillo, V., Lusvarghi, L. and Manfredini, T., Experimental characterisation and numerical modelling of plasma-sprayed composite glass coatings. In *Proceedings of CIEC 9, 9th European Interregional Conference on Ceramics*, ed. A. Negro and L. Montanaro. Torino, 2004, pp. 265–270.
21. Gibson, R. F., *Principles of Composite Material Mechanics*. McGraw-Hill, Singapore, 1994.
22. Pina, J., Dias, A. and Lebrun, J. L., Mechanical stiffness of thermally sprayed coatings and elastic constants for stress evaluation by X-ray diffraction. *Mater. Sci. Eng. A*, 1999, **267**, 130–144.
23. Siebert, B., Funke, C., Vaβen, R. and Stöver, D., Changes in porosity and Young's Modulus due to sintering of plasma sprayed thermal barrier coatings. *J. Mater. Processing Technol.*, 1999, **92–93**, 217–223.
24. Damani, R. J. and Makroczy, P., Heat treatment induced phase and microstructural development in bulk plasma sprayed alumina. *J. Eur. Ceram. Soc.*, 2000, **20**, 867–888.
25. Oliver, W. C. and Pharr, G. M., An improved technique for determining hardness and elastic modulus using load and displacement sensing indentation experiments. *J. Mater. Res.*, 1992, **7**, 1564–1583.
26. Amato, I. and Montanaro, L., Lezioni dal Corso di Scienza e Tecnologia dei Materiali Ceramici, Edizioni Libreria Cortina, Torino, 2000, p. 65 (in Italian).
27. Wang, Z., Kulkarni, A., Deshpande, S., Nakamura, T. and Herman, H., Effects of pores and interfaces on effective properties of plasma sprayed zirconia coatings. *Acta Materialia*, 2003, **51**, 5319–5334.
28. Fernandez, J. E., Rodriguez, R., Wang, Y., Vijande, R. and Rincon, A., Sliding wear of a plasma-sprayed Al_2O_3 coating. *Wear*, 1995, **181–183**, 417–425.
29. Damani, R. J. and Wanner, A., Microstructure and elastic properties of plasma-sprayed alumina. *J. Mater. Sci.*, 2000, **35**, 4307–4318.
30. Westergard, R., Erickson, L. C., Axén, N., Hawthorne, H. M. and Hogmark, S., The erosion and abrasion characteristics of alumina coatings plasma sprayed under different spraying conditions. *Tribol. Int.*, 1998, **31**, 271–279.
31. Killinger, A., Gadow, R. and Li, C., Thermally sprayed functional coatings on glass and glass ceramics substrates for industrial applications. In *Proceedings of CIEC 9, 9th European Interregional Conference on Ceramics*, ed. A. Negro and L. Montanaro. Torino, 2004, pp. 225–230.
32. Bianchi, L., Denoirjean, A., Blein, F. and Fauchais, P., Microstructural investigation of plasma-sprayed ceramic splats. *Thin Solid Films*, 1997, **299**, 125–135.
33. Rohan, P., Neufuss, K., Matejicek, J., Dubsky, J., Prchlik, L. and Holzgartner, C., Thermal and mechanical properties of cordierite, mullite and steatite produced by plasma spraying. *Ceram. Int.*, 2004, **30**, 597–603.

34. Bolelli, G., Cannillo, V., Lusvarghi, L., Manfredini, T., Siligardi, C., Bartuli, C. *et al.*, Plasma-sprayed glass and glass-ceramic coatings on ceramic tiles: microstructure, chemical resistance and mechanical properties. *J. Eur. Ceram. Soc.*, 2005, **25**(11), 1835–1853.
35. Torrecillas, R., Fantozzi, G., de Aza, S. and Moya, J. S., Thermomechanical behaviour of mullite. *Acta Materialia*, 1997, **45**(3), 897–906.
36. Aksel, C., Rand, B., Riley, F. L. and Warren, P. D., Thermal shock behaviour of magnesia-spinel composites. *J. Eur. Ceram. Soc.*, 2004, **24**, 2839–2845.
37. Rangaraj, S. and Kokini, K., Interface thermal fracture in functionally graded zirconia-mullite-bond coat alloy thermal barrier coatings. *Acta Materialia*, 2003, **51**, 251–267.